AIChE WILEY InterScience DISCOVER SOMETHING GREAT

PARTICLE TECHNOLOGY AND FLUIDIZATION

Extension of PIV for Measuring Granular Temperature Field in Dense Fluidized Beds

W. Dijkhuizen, G. A. Bokkers, N. G. Deen, M. van Sint Annaland, and J. A. M. Kuipers
Faculty of Science and Technology, University of Twente, NL-7500 AE Enschede, The Netherlands

DOI 10.1002/aic.11044
Published online November 7, 2006 in Wiley InterScience (www.interscience.wiley.com).

In this work a particle image velocimetry (PIV) technique has been extended to enable the simultaneous measurement of the instantaneous velocity and granular temperature fields. The PIV algorithm has been specifically optimized for dense granular systems and has been thoroughly tested with artificially generated images. The new PIV technique has been successfully applied to a fluidized bed at incipient fluidization conditions in which a single bubble is injected by a jet and to a freely bubbling fluidized bed. The instantaneous spatial distribution of the solids-phase velocity and granular temperature that can be measured with this new technique can be used to validate CFD models for dense granular systems, such as multifluid continuum models using the KTGF (kinetic theory of granular flow) to describe the internal momentum transport in the particulate phase. © 2006 American Institute of Chemical Engineers *AIChE J,* 53: 108–118, 2007

Keywords: particle image velocimetry (PIV), granular temperature, velocity, fluidized bed

Introduction

Large industrial-scale fluidized beds are widely used in the chemical industry because of their excellent heat and mass transfer properties, isothermal conditions throughout the bed, and the possibility of continuous operation. Applications include catalytic cracking of oil, gas-phase polymerization (such as polyethylene and polypropylene), and granulation (such as detergents and fertilizers).

To be able to simulate industrial size equipment, a multiscale modeling approach was presented by Van der Hoef et al.[1] (Figure 1). The basic idea of this strategy is to use lower-level models as well as dedicated experiments to generate closures for key hydrodynamic interactions (such as gas–particle and particle–particle interactions) that are required in higher-level models. At the lowest level, using a lattice–Boltzmann model or an immersed boundary method, closures can be derived for the drag, lift, and virtual mass forces acting on a single particle or clusters of particles.[2] For larger, but still small-scale systems [$<O(10^6)$ particles], the discrete particle model (DPM) can be used, which tracks every particle using Newton's second law of motion. Particle collisions are evaluated with a detailed collision model (see, for example, Bokkers et al.[3]) and closures for the gas–particle interactions also need to be specified to the DPM. Engineering-scale systems can be simulated with a multifluid model (MFM), where all the phases are modeled as interpenetrating continua where the kinetic theory of granular flow (KTGF) is used to account for particle–particle interactions. Finally, for industrial-scale equipment a discrete bubble model (DBM) is used, where the emulsion phase is treated as a continuum and the larger bubbles are treated as discrete elements.

In the KTGF the actual particle velocities are decoupled in a mean and a random fluctuating solids velocity. The magnitude of the fluctuations is characterized by the granular temperature—which is a key parameter in the KTGF. For validation of KTGF-based continuum models the spatial distribution of the granular temperature is particularly required, which can be derived from simulations with the DPM as well as from measurements.

Correspondence concerning this article should be addressed to M. van Sint Annaland at M.vanSintAnnaland@tnw.utwente.nl.

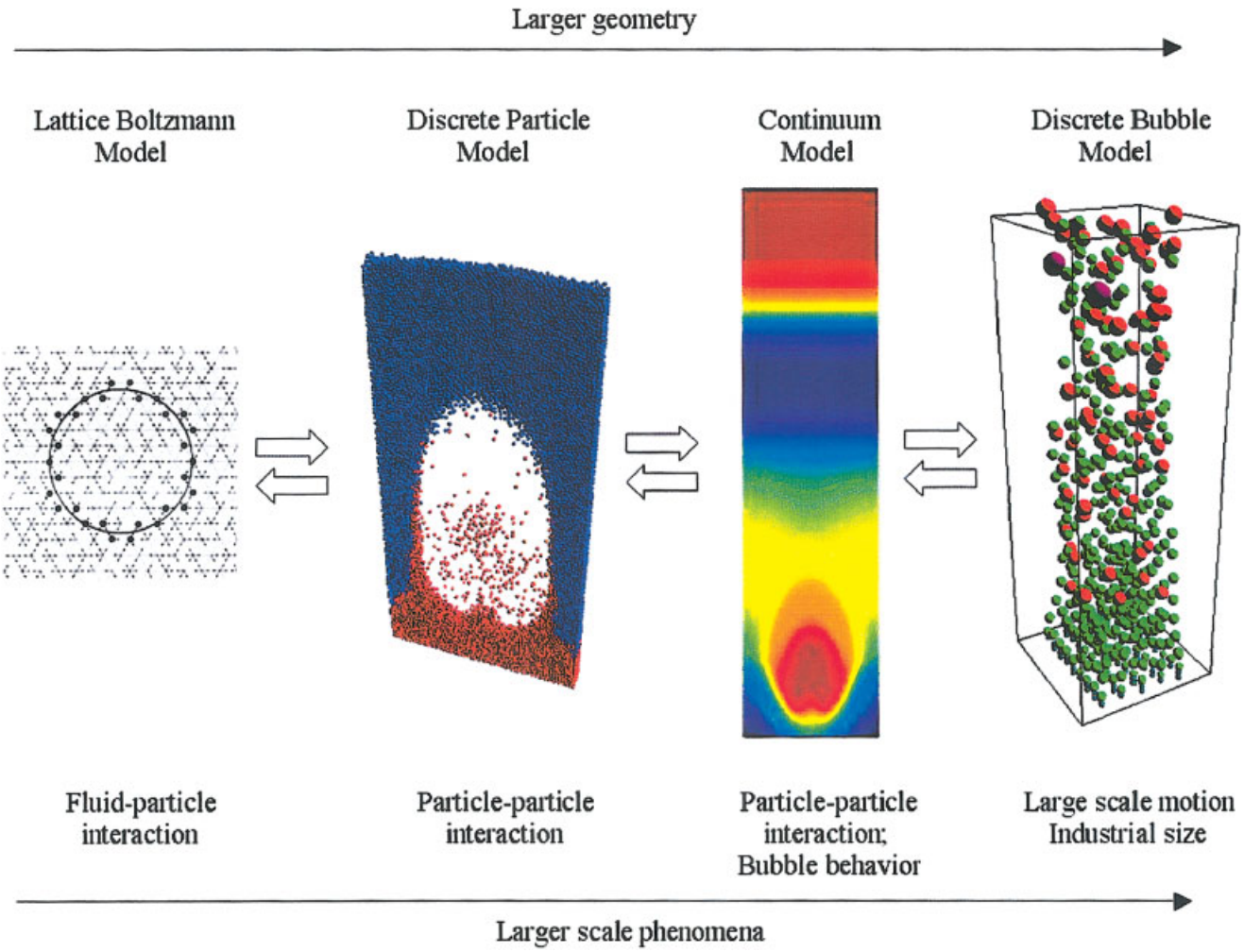

Figure 1. Multilevel modeling strategy for dense gas–solid fluidized beds.[1]

[Color figure can be viewed in the online issue, which is available at www.interscience.wiley.com.]

Despite the fact that so many researchers use the continuum approach based on the KTGF to model fluidized beds, the literature reports only a few studies that focus on the measurement of granular temperature. Cody et al.[4] introduced and validated a novel nonintrusive experimental technique to measure the granular temperature of monodisperse glass spheres at the wall of a fluidized bed. This technique measures the acoustic shot noise excitation of the surface of the fluid bed vessel by random particle impact. Zhang et al.[5] measured particle velocities and particle velocity fluctuations (granular temperature) in riser flow of cohesive (Geldart C) particles using a laser Doppler anemometer (LDA) system. Menon and Durian[6] applied diffusing-wave spectroscopy to measure extremely small velocities and velocity fluctuations in a fluidized bed consisting of small spherical glass beads. More recently, Wildman and Huntley[7] and Wildman[8] used particle tracking velocimetry (PTV) to measure the granular temperature in a vibro-fluidized bed. In this technique the velocity of every single particle is measured and from these data the velocity distribution and the granular temperature can be calculated. The downside of this technique is that for dense systems with fast moving particles a very high frame rate is necessary to keep track of every single particle. Furthermore, the particle tracking technique demands a very high spatial resolution with a correspondingly very small measurement area to obtain precise velocity and granular temperature measurements. Finally, Gidaspow et al.[9] used an optical probe and a CCD (charge-coupled detector) camera to capture the streaks of fast moving particles in a riser flow. From the length of the streaks the velocity of each particle can be calculated and an ensemble of particles (10–30) is used to calculate the granular temperature. However, none of these methods can be used to instantaneously measure the granular temperature in a whole region, which is useful for validation of the KTGF applied to bubbling fluidized beds.

In this work a novel noninvasive technique is presented to directly measure the granular temperature in dense fluidized beds, based on particle image velocimetry (PIV). In the recent past, PIV has already been used to measure the whole-field instantaneous particle velocity field in a fluidized bed[3] and a spout-fluid bed.[10] This article describes the extension of this PIV technique to simultaneously measure the instantaneous velocity and granular temperature fields in dense granular systems.

Theoretical Background

PIV is a nonintrusive technique for the measurement of an instantaneous velocity field in one plane of a flow. In traditional PIV for liquid or gas–liquid flows, the flow is visualized by seeding it with small tracer particles that closely follow the flow. In gas–particle flows, the discrete particles can be readily distinguished, so no additional tracer particles are needed to visualize the particle movement. The front of the bed is illuminated with the use of halogen lamps. A CCD camera is used to record images of the particles in the illuminated plane. Two subsequent images of the flow, separated by a short time delay, Δt, are divided into small interrogation areas. Cross-correlation analysis is then used to determine the volume-averaged displacement, $\bar{s}(\bar{x}, t)$, of the particle images between interrogation areas in the first and second images. Finally, the velocity is found by dividing the displacement by the time delay.

Cross-correlation of digital images

The spatial cross-covariance of two images can be separated in an ensemble mean value $\langle C(x,y)\rangle$ and a random fluctuating term $C'(x,y)$:

$$C(x,y) = \langle C(x,y)\rangle + C'(x,y) = R_D(x,y) + R_C(x,y) + R_F(x,y) + C'(x,y) \quad (1)$$

where R_D represents the displacement peak, R_C is the background correlation, and R_F is the correlation between the mean and fluctuating image intensities. The last two terms can be removed by subtracting the mean intensity from the images before correlating them. The displacement correlation peak can be represented as follows:

$$R_D(x,y) = N_I \cdot F_I(x,y) \cdot F_O \cdot F_T(x,y) \cdot \rho(x,y) \quad (2)$$

in which N_I is the number of particle images in the interrogation area. F_I indicates the loss of correlation arising from in-plane movement of the particles out of the interrogation area. F_O represents the loss of correlation arising from particles leaving the interrogation area perpendicular to the plane.[11] Because the time between two images is very small and the pseudo-2D setup limits the out-of-plane movement of the particles, $F_O \cong 1$. Finally, the function F_T describes the shape of the peak resulting from the particle image properties and $\rho(x, y)$ represents the shape of the peak attributed to the velocity distribution.

Relation between the granular temperature and the displacement peak

After the cross-covariance has been calculated a Gaussian curve is fitted to the displacement peak:

$$R_D(x,y) \sim \exp\left[-(x-x_c)^2/2\sigma_{cc,x}\right] \cdot \exp\left[-(y-y_c)^2/2\sigma_{cc,y}\right] \quad (3)$$

There are several reasons to use a Gaussian peak fit:

(1) The light intensity distribution normal to the measurement plane (z-direction) is approximately Gaussian.

(2) The intensity distribution of a single particle is approximately Gaussian.

(3) The particles have an approximately Gaussian velocity distribution.

Note that (x_c, y_c) represents the center of the correlation peak (average displacement), whereas the width in the x- and y-directions can be expressed as the standard deviations $\sigma_{cc,x}$ and $\sigma_{cc,y}$, respectively. The width of the Gaussian curve is related to the particle diameter and the shape of the velocity distribution. The latter is a function of the granular temperature. To obtain the contribution of the velocity distribution, the particle size contribution F_T has to be eliminated, which can be done by calculating the autocorrelation of both single images and taking the average:

$$F_T[x,y] \sim \exp\left[-(x-x_c)^2/2\sigma_{ac,x}^2\right] \cdot \exp\left[-(y-y_c)^2/2\sigma_{ac,y}^2\right] \quad (4)$$

The velocity profile is also assumed to be Gaussian and can therefore be described as

$$\rho[x,y] \sim \exp\left[-(x-x_c)^2/2\sigma_{d,x}^2\right] \cdot \exp\left[-(y-y_c)^2/2\sigma_{d,y}^2\right] \quad (5)$$

where $\bar{\sigma}_d$ represents the standard deviation in the displacement. Equations 3, 4, and 5 can be combined, yielding the following relations for $\bar{\sigma}_d$:

$$\sigma_{d,x}^2 = \sigma_{cc,x}^2 - \sigma_{ac,x}^2 \quad (6)$$

$$\sigma_{d,y}^2 = \sigma_{cc,y}^2 - \sigma_{ac,y}^2 \quad (7)$$

The definition of the granular temperature, written in terms of displacement, is given by Eqs. 8 and 9. For a Gaussian velocity profile the average square displacement can be easily related to the standard deviation:

$$\theta_x = m_n\left\langle (v_x - \langle v_x\rangle)^2\right\rangle = \frac{m_n}{(M\Delta t)^2}\left\langle (x-x_c)^2\right\rangle = \frac{m_n}{(M\Delta t)^2}\ \sigma_{d,x}^2 \quad (8)$$

$$\theta_y = m_n\left\langle (v_y - \langle v_y\rangle)^2\right\rangle = \frac{m_n}{(M\Delta t)^2}\left\langle (y-y_c)^2\right\rangle = \frac{m_n}{(M\Delta t)^2}\ \sigma_{d,y}^2 \quad (9)$$

where m_n is the mass of particle class n and M is the camera magnification. Finally, the overall granular temperature is averaged in two dimensions:

$$\theta = \frac{\theta_x + \theta_y}{2} \quad (10)$$

Interpolation of the displacement peak

To calculate the standard deviation of the correlation peak, a Gaussian curve is fitted to the correlation signal. Most PIV software uses a three-point Gaussian fit to find the displacement with subpixel accuracy. This works well for small (tracer) particles, where the correlation peak will generally be in the order of three pixels wide. However, with particles that are used in lab-scale fluidized beds and in combination with modern camera equipment, particle images with diame-

Table 1. Test Settings for the Displacement Error

Variable	Description	Tested Range	Step Size
d_t	Particle image diameter	2–20 px	2 px
N_I	Particle image density	5–75	5
x_c	x-displacement	0–0.5 px	0.05 px
y_c	y-displacement	0–0.5 px	0.05 px

ters up to 10 pixels are not uncommon. In this case the interpolation should be extended to include more than three points to enhance the attainable measurement accuracy of the granular temperature and to exclude noise.

To exclude random correlation and secondary peaks only points with a correlation signal higher than 50% of the peak height are included in the interpolation. This is especially important in dense granular systems, where the interparticle spacing can be much smaller than the particle image size. Subsequently, the natural logarithm is taken, reducing the Gaussian peak to a parabola (Eq. 11). The same is done for the y-direction:

$$\ln R[x, y_m] = \ln(c_0) - \frac{(x - x_c)^2}{2\sigma_x^2} = c_1 + c_2 x + c_3 x^2$$

$$c_1 = \ln(c_0) - \frac{x_c^2}{2\sigma_x} \qquad c_2 = \frac{x_c}{\sigma_x^2} \qquad c_3 = \frac{1}{2\sigma_x^2} \tag{11}$$

Finally, Eq. 11 can be fitted using a least-square approximation (Eq. 12). Once the coefficients c_1, c_2, and c_3 are known the average displacement and the standard deviation can be easily calculated.

$$A^T A \cdot c = A^T \cdot b \qquad A = \begin{bmatrix} 1 & x_1 & x_1^2 \\ \cdots & \cdots & \cdots \\ 1 & x_n & x_n^2 \end{bmatrix}$$

$$A^T = \begin{bmatrix} 1 & \cdots & 1 \\ x_1 & \cdots & x_n \\ x_1^2 & \cdots & x_n^2 \end{bmatrix} \qquad b = \begin{bmatrix} \ln R[x_1, y_m] \\ \cdots \\ \ln R[x_n, y_m] \end{bmatrix} \qquad c = \begin{bmatrix} c_1 \\ c_2 \\ c_3 \end{bmatrix} \tag{12}$$

Testing of the Method with Synthetic Images

The PIV software originally developed by Westerweel[13] was modified to calculate and output the standard deviation of the correlation peak, as described in the previous section. A least-square approximation was incorporated, so that broad displacement peaks can be accurately interpolated. As a first step artificially created particle images with prescribed average velocities and granular temperatures are used to test the precision as a function of different parameters, such as the particle diameter and the particle image density.

Image-generation software

For testing purposes an image-generation program was written. With this program pairs of synthetic images can be made, where the particle image size and density can be varied. Using the positions of the particles on the first image, the ensemble of particles can be moved according to a Gaussian velocity distribution and a second image can be created. In the first image the particles are placed at random positions, while ensuring that the particles do not overlap. This can be accomplished by introducing the particles one by one, checking for overlap, and retrying to place the particle at a new position until the particle no longer overlaps with other particles.

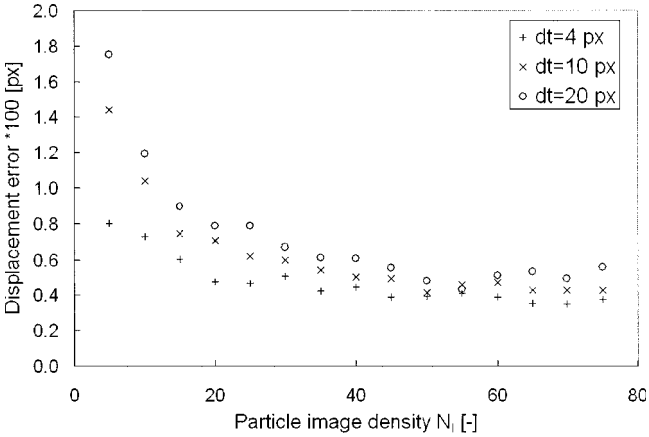

Figure 2. Influence of the particle image density on the displacement error for a uniform particle displacement.

It can be seen that for all three particle image diameters (d_t) the error decreases asymptotically to approximately the same value when the number of particles is increased.

Uniform particle velocity

First of all, the new least-squares interpolation method is tested using a uniform velocity field in the x- and y-directions. For each combination of particle image density and particle size, the x- and y-velocities are varied as indicated in Table 1.

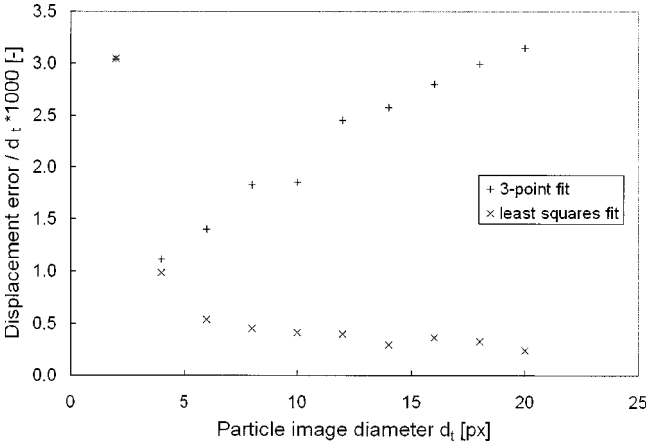

Figure 3. Influence of the particle image diameter on the relative displacement error, using perfectly Gaussian test images and a uniform particle displacement.

The error is an average of different combinations of x- and y-displacements.

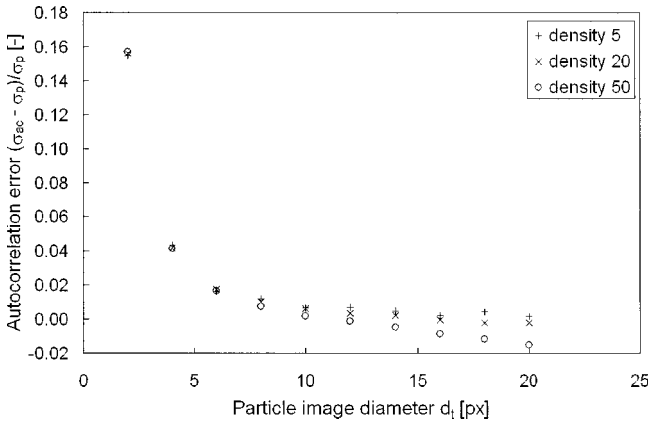

Figure 4. Difference between the standard deviation obtained by autocorrelation (σ_{ac}) and the theoretical value ($\sigma_p = 2\sqrt{2}d_t$) as a function of the particle image density.

It can be seen that for sufficiently large particles there is a very good agreement.

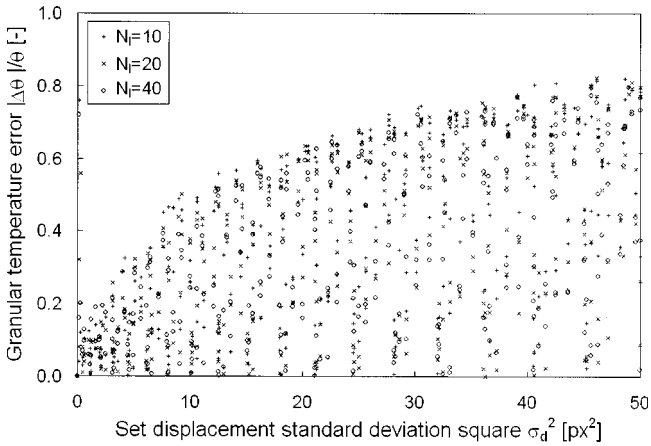

Figure 5. Scatterplot of the relative error in the granular temperature from the computer-generated images as a function of the specified standard deviation in the displacement.

It can be seen that the points are spread evenly over the graph and the number of particles (N_I) does not affect the error.

In Figure 2 the displacement errors as a function of the particle number density are compared for three different particle image diameters d_t using the new least-squares peak fit. It can be seen that the error decreases asymptotically with increasing N_I. At lower particle image densities, the velocity is systematically overestimated because the velocity bias correction works properly only for a statistically sound number of particles. At higher particle image densities, the root-mean-square (RMS) displacement error hardly depends on the number of particles, as expected from theory, because of the uniform particle displacement.[12] The results for the RMS displacement error, normalized by the particle image diameter, at an image density of 50 particles are shown in Figure 3. A comparison between both interpolation methods shows that for larger particle images the least-squares method is superior. The minimum number of points for interpolation is three, for which the least-squares method reduces to an exact three-point fit commonly used in PIV. This is confirmed by the results for a particle image diameter of two pixels. Note that a Gaussian particle image with a standard deviation σ_p when correlated yields a Gaussian correlation with a width of $\sqrt{2}\sigma_p$. Finally, the use of autocorrelation for determination of the particle size correction has been analyzed for different particle velocities. Figure 4 shows the difference between the standard deviation obtained from autocorrelation (σ_{ac}) and the theoretical value [$\sigma_p = d_t/(2\sqrt{2})$]. It can be concluded that there is a good agreement for sufficiently large particles, which supports the use of an approximately Gaussian particle shape.

Gaussian velocity profile

As a second test, a Gaussian velocity profile was applied to verify the method for particles with a specified standard deviation in the x- and y-directions (see Table 2). With this test it can be verified whether the software reproduces the granular temperature as specified in the generation of the test images. From Figure 5 (see below), it can be discerned that for various combinations of standard deviations in the x- and y-directions, the error in the granular temperature does not depend on the particle image density. Furthermore, the average error increases from roughly 10% for low values to roughly 40% for high values of the granular temperature. The maximum granular temperature encountered in the setup used in this work resembles a standard deviation of 20 px^2. From Figure 5 it can be concluded that for this value of the squared standard deviation the average error is roughly 30%. It is noted that in the pseudo-2D experiments the particle movement and therefore also the granular temperature is oriented mainly in one direction, which further substantially reduces the error.

Optimization of the Method with Real Particles

PIV settings

Before experiments are done the size of the interrogation areas has to be selected, which has a profound effect on the range of granular temperatures that can be determined. In

Table 2. Test Settings for the Gaussian Velocity Profile

Variable	Description	Tested Range	Step Size
d_t	Particle image diameter	10 px	—
N_I	Particle image density	10–40	10
x_c, y_c	x- and y-displacement	0.5 px	—
σ_x, σ_y	x- and y-standard deviation	0–10.0 px^2	0.5 px^2

Table 3. PIV Settings for the Experiments

Variable	Description	Value for a particle diameter of 1.5 mm	Value for a particle diameter of 2.5 mm
M	Image magnification	4400 px/m	4400 px/m
N_I	Particle image density	100	100
d_t	Particle image diameter	7 px	11 px
D_I	Interrogation area size	72 × 72 px^2	120 × 120 px^2

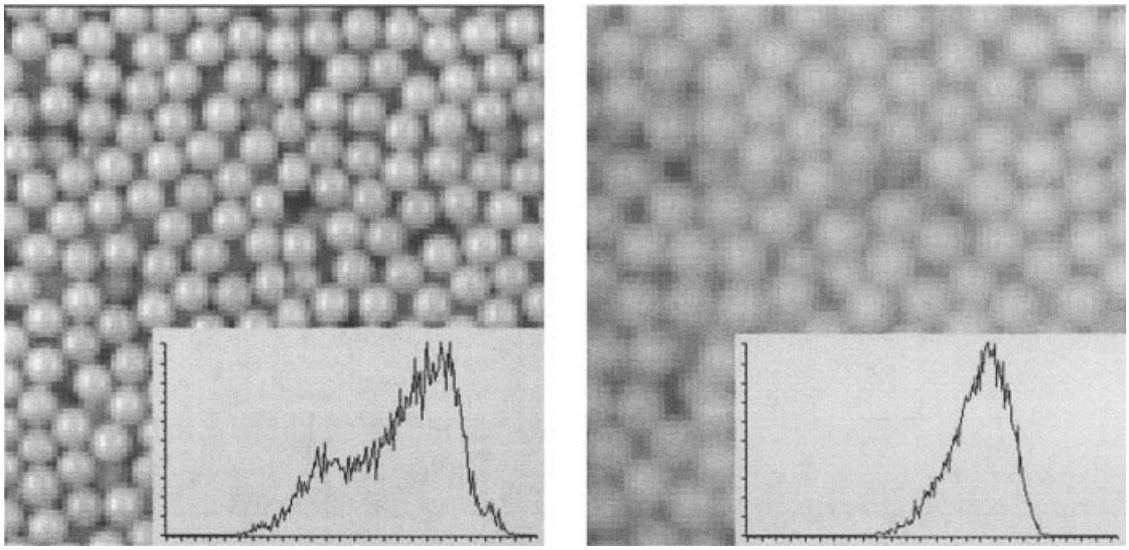

Figure 6. Examples of direct (left) and indirect (right) lighting of the particles and the corresponding intensity distribution (not on the same scale).

Direct is better than indirect lighting because of its superior contrast ratio, which improves the correlation.

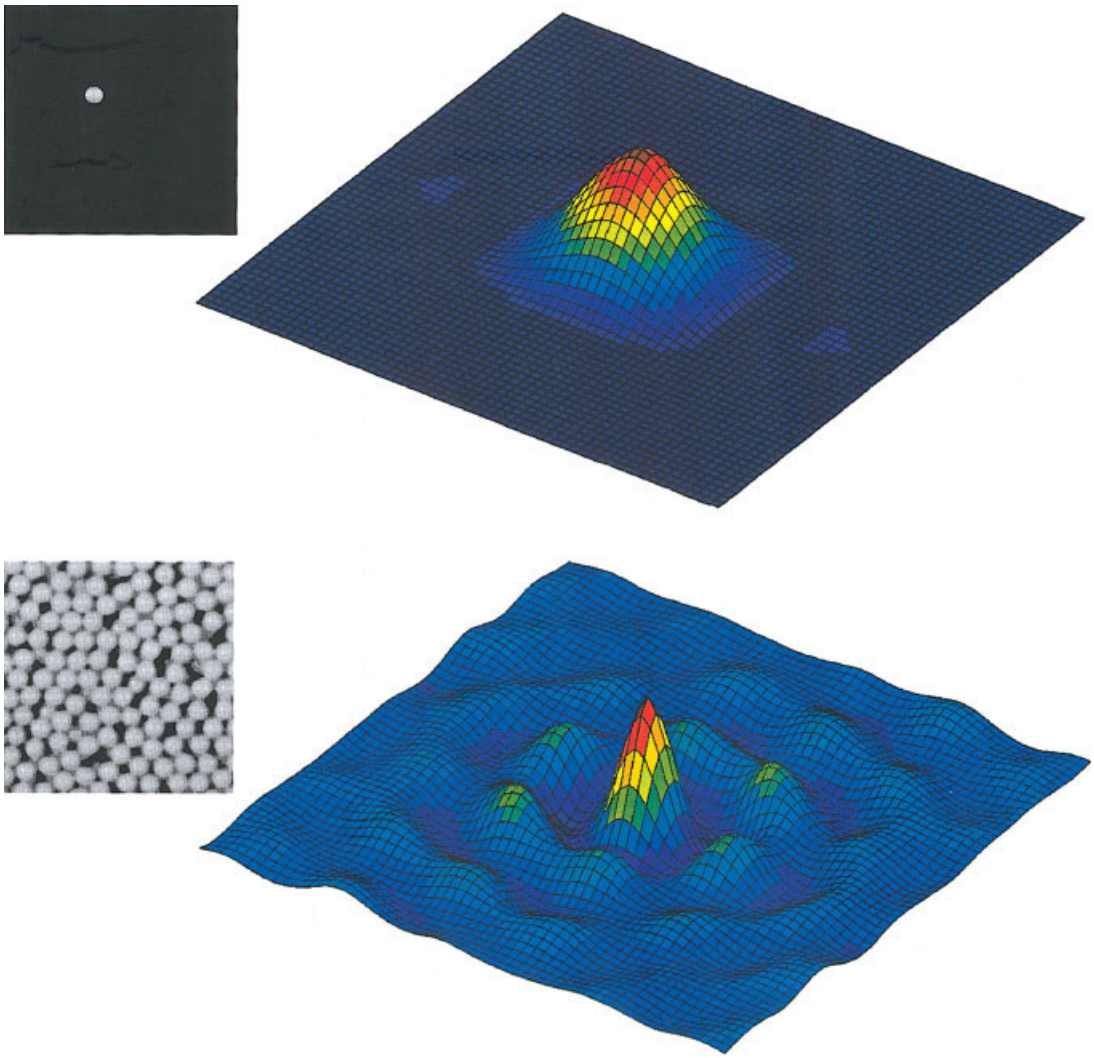

Figure 7. Particle images and the corresponding autocorrelation signal for dilute (top) and dense (bottom) systems.

[Color figure can be viewed in the online issue, which is available at www.interscience.wiley.com.]

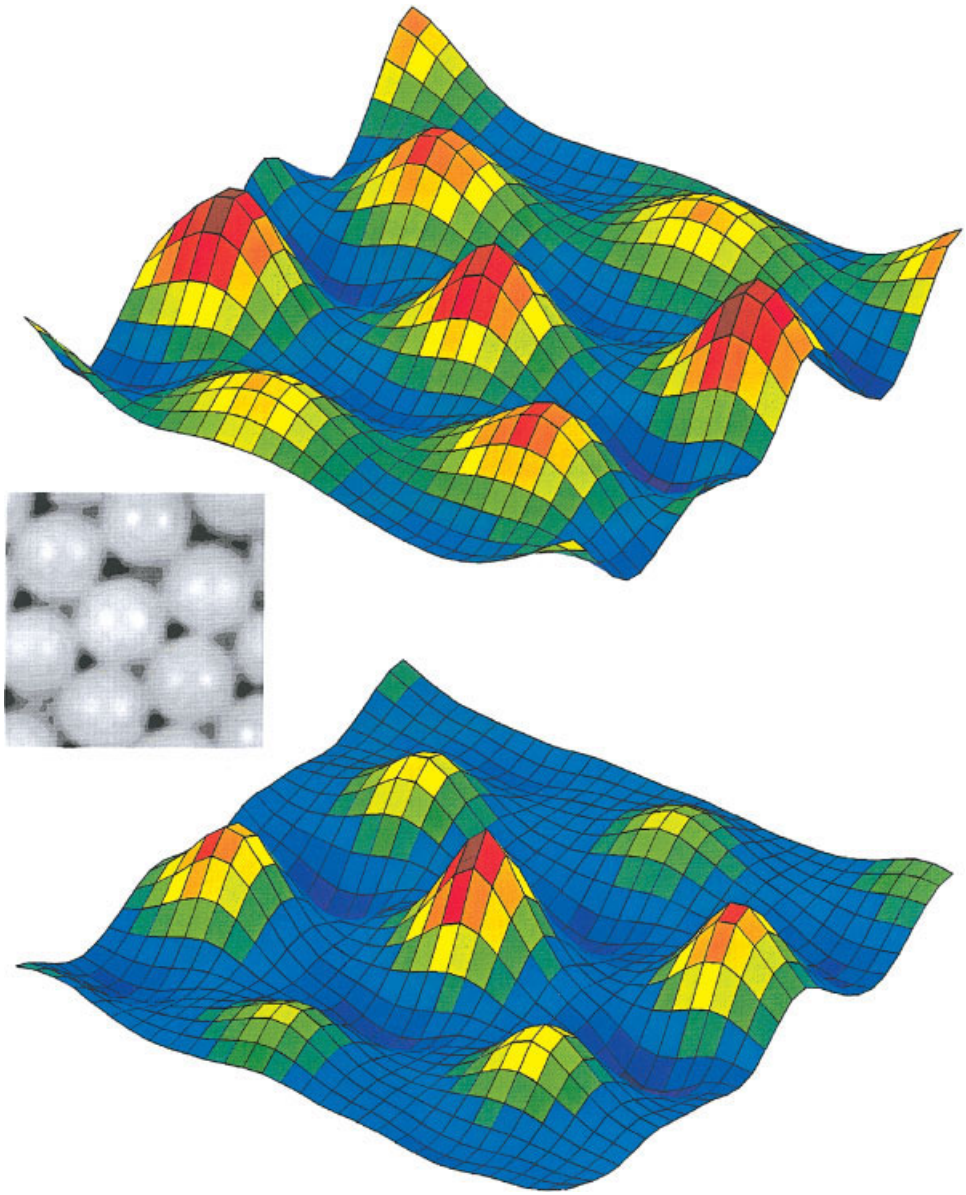

Figure 8. Correlation of a structured particle packing without (top) and with zero-padding (bottom).

[Color figure can be viewed in the online issue, which is available at www.interscience.wiley.com.]

general with a larger interrogation area a higher granular temperature range can be measured because there are more particles in each interrogation area. Tests have shown that the accuracy of the granular temperature measured is dominated by the quality of the velocity distribution. Therefore the interrogation size was chosen such that an average particle image density of 100 was obtained, to ensure sufficient accuracy also in less dense areas. The resulting settings are summarized in Table 3.

Direct lighting vs. indirect lighting

The way in which particles are illuminated is very important for the quality of the correlation signal. Direct lighting has the advantage of higher contrast and therefore the particles can be separated more easily (Figure 6, left). This particularly improves the separation of the correlation peak from the random correlation. The use of indirect lighting has been investigated, which resulted in a more pronounced Gaussian peak of the particle intensity distribution, although unfortunately the contrast is appreciably reduced (Figure 6, right). Thus, direct lighting was used in all experiments.

Autocorrelation tests with real particles

To verify the method for true experimental images, the autocorrelation signal of a single experimental particle image was determined (Figure 7, top). It can be seen that the shape of the correlation is distinctively Gaussian and it is surrounded by a correlation of zero value. Subsequently, the

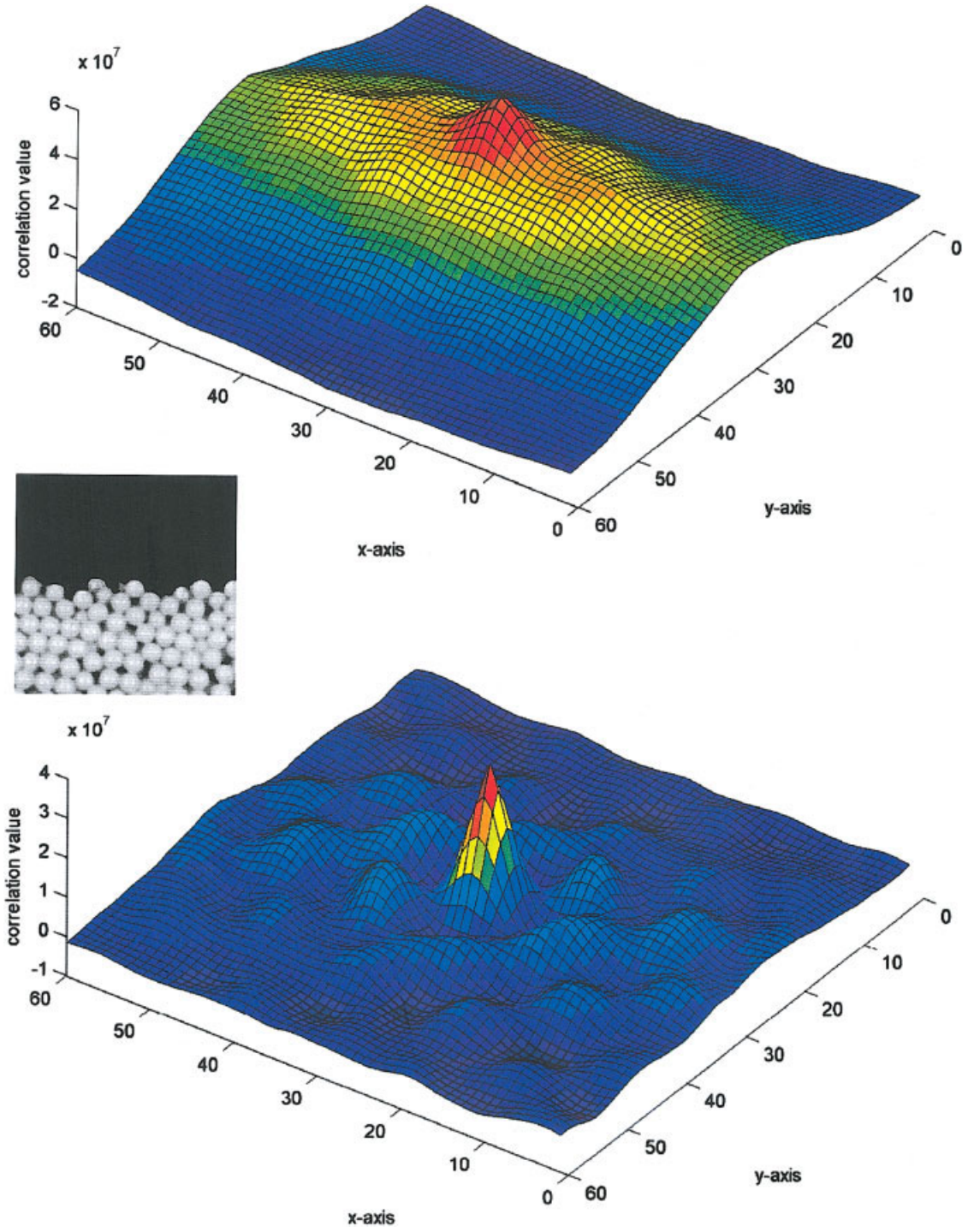

Figure 9. Correlation of an inhomogeneous interrogation area before correction (top) and after correction (bottom).

[Color figure can be viewed in the online issue, which is available at www.interscience.wiley.com.]

autocorrelation signal of a dense region of the same particles was determined (Figure 7, bottom). The shape of the correlation peak is again nicely Gaussian. However, the peak is much narrower than that for the single particle. This is caused by the normalization of the mean image intensity in the correlation. For the single particle the mean image intensity is almost zero (black), whereas for the dense system it is approximately the mean intensity of the particle itself (gray). This effectively reduces the peak width and height, but fortunately does not impair the shape of the correlation peak.

When particles are arranged in a structured packing, the secondary correlation peaks may become dominant (Figure 8, top). This is caused by the periodic nature of the fast Fourier transformation (FFT) used to calculate the correlation. In

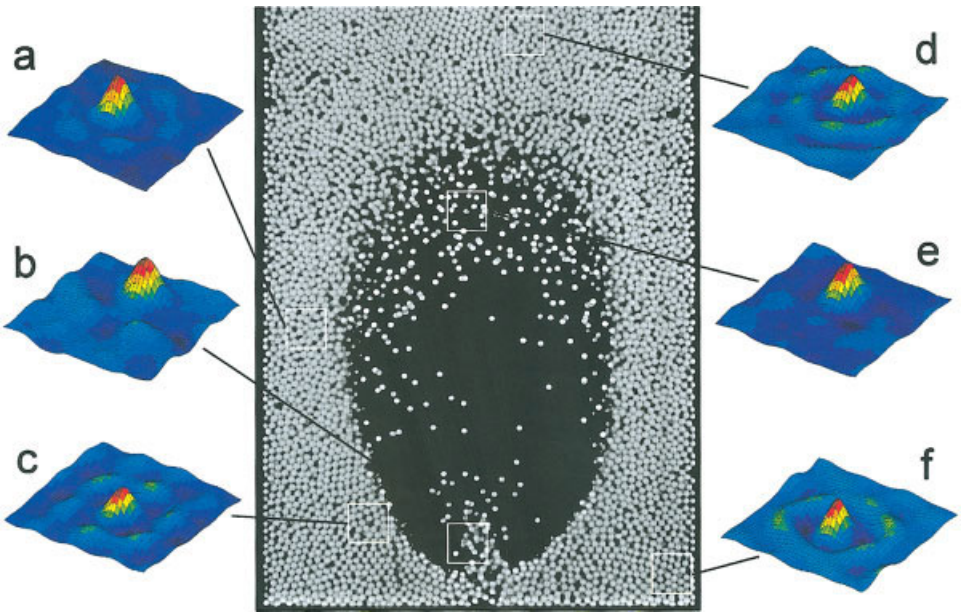

Figure 10. Image cross-correlation at different locations in a single bubble experiment, using 2.5 mm particles in a 15 cm wide fluidized bed.

[Color figure can be viewed in the online issue, which is available at www.interscience.wiley.com.]

principle the exact correlation can be calculated directly according to the definition of the cross-correlation, although this is very time consuming. To fix the periodic issues associated with the use of a FFT, zero-padding is used,[13] which places a black border with a width of 50% of the interrogation area around the picture. It is important to apply zero-padding only *after* normalization of the intensity, to avoid the possibility that the black border will give a correlation with itself. The result is given in Figure 8 (bottom) and it can be seen that the detectability of the main peak has improved significantly.

Table 4. Experimental Settings

Bed	Small	Large
Width	0.15 m	0.30 m
Depth	0.015 m	0.015 m
Height	1.0 m	1.0 m
Initial bed height	0.18 m	0.22 m
Front plate	glass	glass
Back plate	polycarbonate	glass
Left and right wall	aluminum	aluminum
Porous plate average pore size	10 μm	10 μm
Porous plate thickness	1.5 mm	1.5 mm
Jet width	0.01 m	0.015 m
Particles	**Small**	**Large**
Material	glass	glass
Diameter	1.5 mm	2.5 mm
Density	2526 kg/m^3	2526 kg/m^3
Minimum fluidization velocity (experimentally obtained)	0.87 m/s	1.31 m/s
Collision Parameters	**Particle–Particle**	**Particle–Wall**
Normal restitution	0.97 $\pm$ 0.01	0.97 $\pm$ 0.01
Friction	0.10 $\pm$ 0.01	0.09 $\pm$ 0.01
Tangential restitution	0.33 $\pm$ 0.05	0.33 $\pm$ 0.05

Another problem arises when we look at the interface of a particle assembly to an empty region, for instance at the top of the fluidized bed or at the bubble interface. Because the image is normalized using the average image intensity, the black background will correlate with itself just as strongly as the particles. The resulting correlation therefore has a wide ridge on top of which the Gaussian peak is located (Figure 9, top). Apparently, a homogeneous particle distribution is required for the image normalization to work properly. However, this is often not the case when granular systems are concerned. Therefore, a modification was devised to cancel the correlation of the background with itself. First of all, the background intensity is subtracted from the image, so that all of the background is really black. Secondly, pixels with intensity zero are not normalized in this procedure, effectively switching off their contribution to the correlation. The improvement of the correlation peak resulting from this procedure for the same inhomogeneous region is evident from Figure 9 (bottom).

Cross-correlation tests with real particles

Finally, two pictures from a single-bubble experiment in a small lab-scale fluidized bed using 2.5 mm particles are used to test the method in a realistic environment (Figure 10). From the results it can be seen that all the cross-correlation peaks at different locations around the bubble are indeed Gaussian, as assumed, even for nonideal particles and lighting. Also it can be seen that the extended interpolation routine based on more than three points is an important improvement.

Now that the developed method has been thoroughly tested and optimized, it can be used to measure the particle velocity field and the granular temperature profiles inside lab-scale fluidized beds. First of all, the idealized case where a single

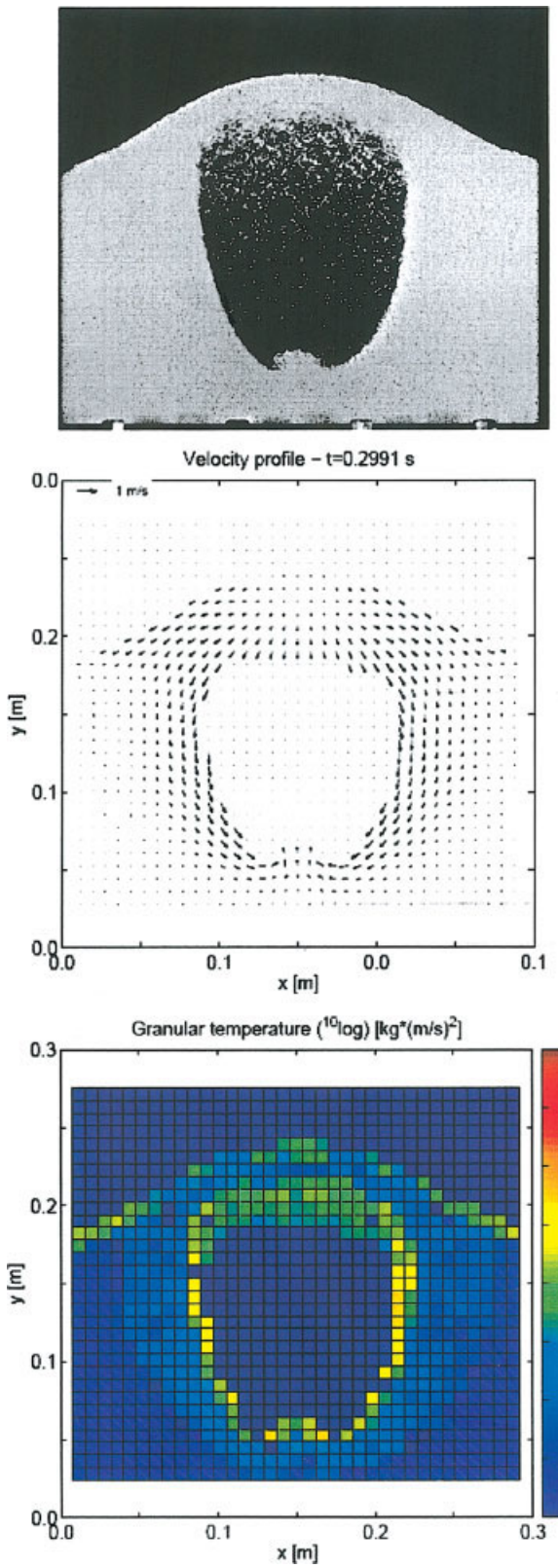

Figure 11. Single-bubble experiment for 1.5 mm particles in a 30 cm fluidized bed.

[Color figure can be viewed in the online issue, which is available at www.interscience.wiley.com.]

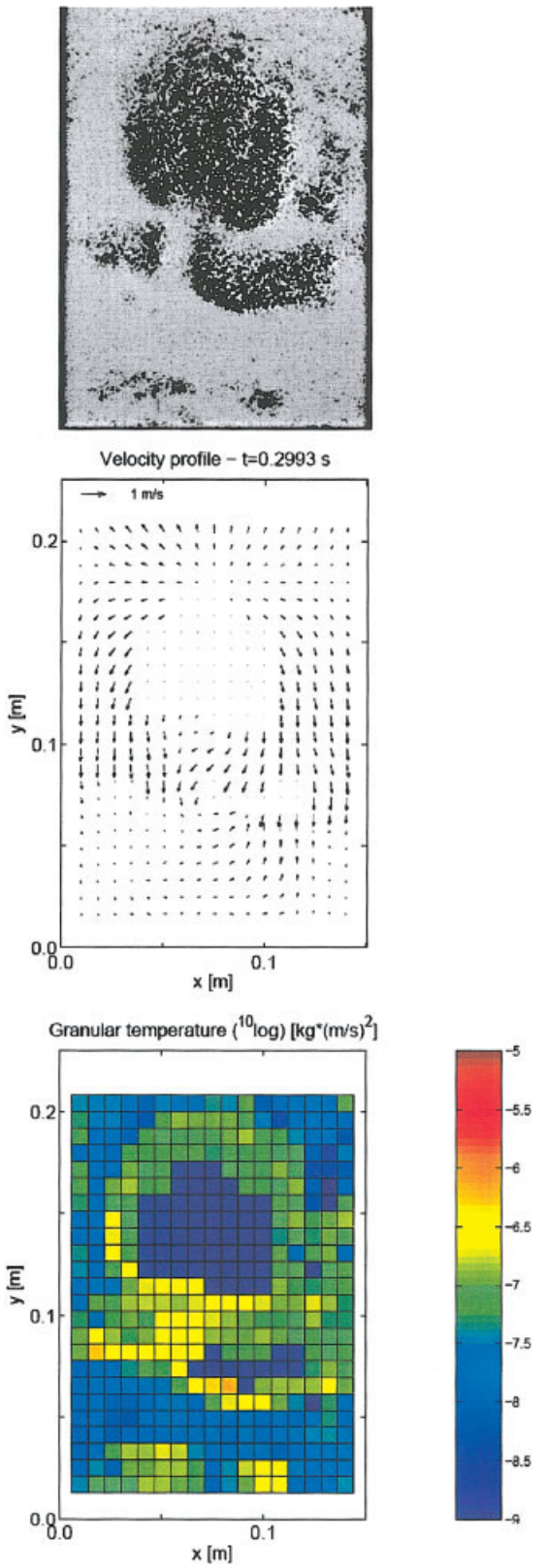

Figure 12. Freely bubbling experiment for 1.5 mm particles in a 15 cm fluidized bed.

[Color figure can be viewed in the online issue, which is available at www.interscience.wiley.com.]

bubble is injected into a fluidized bed at incipient fluidization conditions is studied. Second, a freely bubbling bed is studied, where the bubbles are formed in situ.

Single-Bubble Experiment. The single-bubble experiments were carried out in a fluidized bed with a 30 cm width containing 2.5 mm particles (bed height at incipient fluidization conditions 0.22 m). The bed was kept at minimum fluidization conditions, whereas single bubbles were injected by switching on a 20 m/s jet for 150 ms. The settings for this experiment are shown in Table 4.

In Figure 11 the high-speed images as well as the velocity and granular temperature profiles are given. From the first snapshot, showing the bed without movement, a small uniform (noise) granular temperature in the order of 10^{-9} kg m^2 s^{-2} was found, which can be related to random correlation and the 50 Hz frequency of the lights. In the subsequent snapshots, as the bubble rises in the fluidized bed, the highest granular temperatures are found in the vicinity of the bubble, typically about $10^{-6.5}$ kg m^2 s^{-2}. The second snapshot shows that the more or less uniform expansion of the bed above the bubble results in a low granular temperature. Also, when the bubble has passed, the granular temperature immediately drops down to its initial value, as shown in the last snapshot.

Freely Bubbling Experiment. To investigate whether the method is capable of dealing with systems where there is more vigorous mixing, a freely bubbling experiment was conducted using the same 1.5 mm particles in a 15 cm fluidized bed with a superficial gas velocity of 1.5 m/s. The results are shown in Figure 12.

From the freely bubbling experiments it can be discerned that, as in the single-bubble experiments, the highest granular temperatures are found in the vicinity of the bubbles, even around very small bubbles. The level of the granular temperature around the bubbles is quite comparable with the levels encountered in the single-bubble experiment. The larger bubbles in the freely bubbling case show an even higher granular temperature in their wake. The granular temperature gradient from the bubble surface to the dense phase is again quite high.

Conclusions

In this work the PIV method has been optimized for application to granular media and extended to simultaneously measure the local instantaneous granular temperature. The new method was tested with artificially generated images to assess the effects of particle image size and density. It was found that for higher particle image densities, the error in the velocity and granular temperature decreases. A least-squares fit has been implemented to interpolate broad correlation peaks more accurately than with a standard three-point Gaussian fit.

Tests with real particles in the experimental setup revealed that direct lighting gave better results than indirect lighting because of a higher contrast. Zero-padding was applied to the images to improve the correlation, especially for inhomogeneous areas. Correlation of different regions in a single-bubble experiment showed that good correlation results can be obtained throughout the fluidized bed.

Finally, the experimental method was demonstrated for a single bubble injected into a bed at incipient fluidization conditions and a freely bubbling fluidized bed. Both experiments show that the highest granular temperatures prevail around the bubbles and that the granular temperature quickly returns to virtually zero when a bubble has passed.

Acknowledgments

The authors thank Prof. Dr. Ir. J. Westerweel from the Technical University of Delft for allowing us to use the code of his PIV software and the Dutch Polymer Institute for the financial support of this work.

Literature Cited

1. van der Hoef MA, van Sint Annaland M, Kuipers JAM. Computational fluid dynamics for dense gas–solid fluidized beds: A multi-scale modeling strategy. *China Particuol.* 2005;3:69–77.
2. van der Hoef MA, Beetstra R, Kuipers JAM. Lattice Boltzmann simulations of low-Reynolds-number flow past mono- and bidisperse arrays of spheres: Results for the permeability and drag force. *J Fluid Mech.* 2005;528:233–254.
3. Bokkers GA, van Sint Annaland M, Kuipers JAM. Mixing and segregation in a bidisperse gas-solid fluidised bed: A numerical and experimental study. *Powder Technol.* 2004;140:176–186.
4. Cody GD, Goldfarb DJ, Storch GV Jr, Norris AN. Particle granular temperatures in gas fluidized beds. *Powder Technol.* 1996;87:211–232.
5. Zhang Y, Yang Y, Arastoopour H. Electrostatic effect on the flow behaviour of a dilute gas/cohesive particle flow system. *AIChE J.* 1996;42:1591.
6. Menon N, Durian DJ. Particle motions in a gas-fluidized bed of sand. *Phys Rev Lett.* 1997;79:3407–3410.
7. Wildman RD, Huntley JM. Novel method for measurement of granular temperature distributions in two-dimensional vibro-fluidised beds. *Powder Technol.* 2000;113:14–22.
8. Wildman RD. Measurement of the first and second moments of the velocity distribution in two-dimensional vibro-fluidised beds. *Powder Technol.* 2002;127:203–211.
9. Gidaspow D, Jung J, Singh RK. Hydrodynamics of fluidization using kinetic theory: An emerging paradigm. 2002 Flour-Daniel lecture. *Powder Technol.* 2004;148:123–141.
10. Link JM, Zeilstra C, Deen NG, Kuipers JAM. Validation of a discrete particle model in a 2D spout-fluid bed using non-intrusive optical measuring techniques. *Can J Chem Eng.* 2004;82: 30–36.
11. Keane RD, Adrian RJ. Theory of cross-correlation analysis of PIV images. *Appl Sci Res.* 1992;49:191–215.
12. Westerweel J. Fundamentals of digital particle image velocimetry. *Meas Sci Technol.* 1997;8:1379–1392.
13. Westerweel J. *Digital Particle Image Velocimetry—Theory and Applications.* Delft, The Netherlands: Delft Univ. of Technology; 1993.

Manuscript received Jun. 21, 2006, and revision received Aug. 31, 2006.